

Bumpy Power Spectra and Galaxy Clusters

Alexander Knebe¹, Ranty R. Islam², and Joseph Silk²

¹*Theoretical Physics, Keble Road, Oxford OX1 3NP, UK*

²*Astrophysics, Keble Road, Oxford, OX1 3RH, UK*

Received ...; accepted ...

ABSTRACT

The evolution of the abundance of galaxy clusters is not a reliable measure of Ω if there are features on scales of a few Mpc in the primordial power spectrum. Conversely, if we know the cosmological model parameters from other measurements, the cluster abundance evolution permits us to probe features in the power spectrum that are in the nonlinear regime at the present epoch, and hence difficult to discern directly from current epoch measurements.

We have investigated the influence of an artificially introduced Gaussian feature on an otherwise unperturbed SCDM power spectrum on scales corresponding to $k \sim 0.4 - 0.8 \text{ hMpc}^{-1}$. Using these modified spectra as an input to cosmological N -body simulations, we are able to show that in terms of the cluster abundance evolution, a SCDM model displays characteristics similar to an OCDM model. However, strong modifications would also be visible at a redshift $z = 0$ in the dark matter power spectrum whereas minor alterations to the usual SCDM spectrum are washed away by non-linear evolution effects. We show that alterations to the dark matter power spectrum like those presented in this paper do not leave any imprint in the present density fluctuation spectrum and the velocity distribution of galaxy clusters; nearly all models agree with each other and do not coincide with our fiducial OCDM model, respectively. We therefore conclude that features with characteristics such as discussed here might not be detectable using observations of the galaxy power spectrum, the local cluster abundance or the large-scale velocity field as measured by the velocity distribution of galaxy clusters.

The only quantity that shows a pronounced difference at the present epoch between our models under investigation is the halo-halo correlation function which appears to be strongly biased with respect to an unmodified SCDM model. This is due to a lack of power on certain scales which subsequently modifies the relative amplitude of high- and low- k waves. Apart from observations of the evolution of cluster abundance, measurements of the Lyman α forest at high redshift could put constraints on possible features in the power spectrum, too.

Key words: large scale structure – cosmology: theory – cosmology: large scale structure of Universe

1 INTRODUCTION

The distribution of matter on large scales in the Universe is supposed to have evolved by gravitational interactions from seeds originating in quantum fluctuations that were stretched to cosmological dimensions by inflation. Ordinarily, this initial spectrum of fluctuations is assumed to be a featureless power law. This requires the least number of parameters and is produced in the simplest models of inflation. However, different observations, such as cluster redshift surveys (Einasto et al. 1997) and galaxy surveys (Hamilton & Tegmark 2000, Gaztanaga & Baugh 1998, Broadhurst et al. 1990) reveal possible traces of features in

the matter power spectrum. In addition, a lower than expected second peak in the CMB spectrum as measured by BOOMERANG (Lange et al. 2001) appears to be incompatible with the simplest models of cold dark matter and a scale invariant primordial spectrum.

While the results, particularly from the surveys are still not beyond statistical doubt, a genuine feature(s) in the primordial spectrum cannot be ruled out. Several mechanisms have been proposed that could generate features in the primordial spectrum during the epoch of inflation. They commonly involve an extension of the simplest one field inflation model, e.g. by coupling the inflaton to a massive particle (Chung et al. 1999) or considering two-field inflation

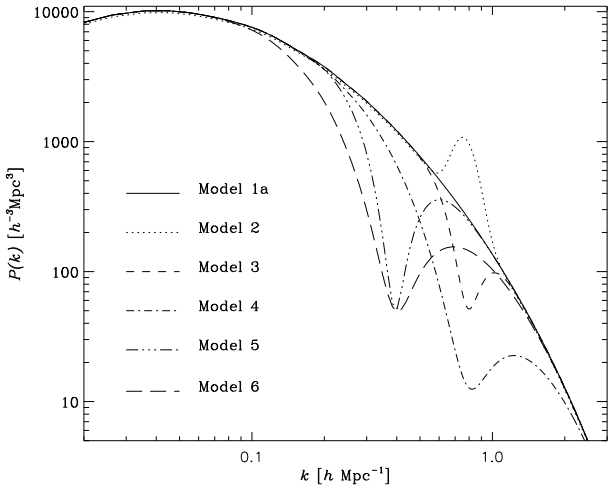


Figure 1. CDM input spectra at redshift $z = 0$.

(Lesgourges, Polarski & Starobinsky 1998). There are also more exotic ideas (see e.g. Martin, Riazuelo & Sakellariadou 1999). Another idea proposed is to Taylor expand the primordial power spectrum to include higher order terms that account for a running spectral index (Lidsey et al. 1997, Hannestad, Hansen & Villante 2000). The latter is able to introduce a very broad negative or positive bend into the power spectrum.

While possibly providing a motivation for observed features on a specific scale (i.e. scales of about 100 Mpc), the inflationary mechanisms proposed appear in principle capable of producing features on other scales as well. Here we examine the effect of primordial features on smaller scales $k \sim 0.4 - 0.8 \text{ hMpc}^{-1}$, where due to (the onset of) non-linear evolution and the problem of biasing, a connection with the primordial spectrum is much harder to establish. We have previously examined the effects of such bumpy power spectra on the cosmic microwave background (Griffiths, Silk and Zaroubi 2001).

In Section 2 we will present the modifications applied to an otherwise unperturbed SCDM power spectrum. These spectra were then used as input to cosmological N -body simulations as described in Section 3. Section 4 deals with the complete analysis of these simulations with respect to the evolution of the power spectrum, velocity statistics, the masses of galaxy clusters, the halo-halo correlation function, and density profiles for a selection of halos. In Section 5 we try to link our numerical results to analytical prediction mainly based on the Press-Schechter theory (Press & Schechter 1974). We close with a discussion of our main results in Section 6.

2 THE POWER SPECTRA

We focus our attention on an SCDM model with parameters as given in Table 1. Although in this paper we are looking at properties of clusters and particularly their abundance evolution, we decided to use only COBE-normalised spectra with spectral index $n = 1$ for modifications. This is because the features we add to the spectra are on scales that at the

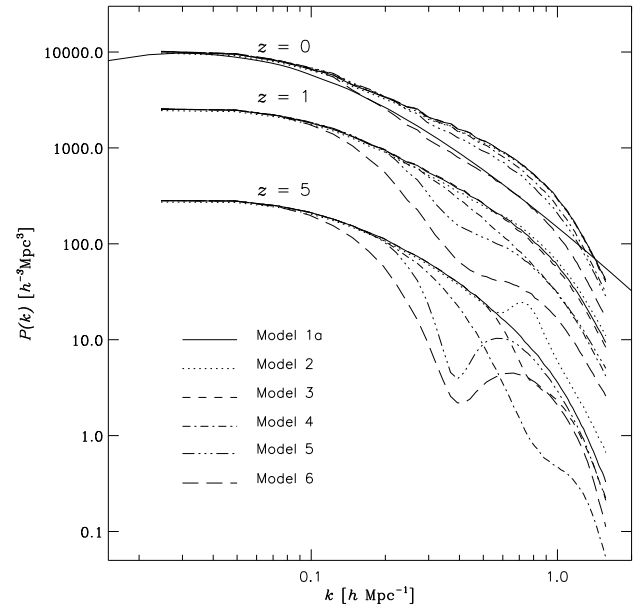


Figure 2. Evolution of CDM spectra.

present time are subject to non-linear evolution and thus are expected to lead to a deviation from the $\sigma_8 - \Omega$ relation (Eke et al. 1996) that would otherwise be used to cluster-normalise the spectra. We also focused our attention mostly on negative amplitude features – or dips – in the spectrum of SCDM models. In addition to the significance of features for structure evolution on relatively small scales, dips will reduce the overall power in the spectrum, pushing the normalisation and possibly other properties towards what is expected in OCDM models.

The corresponding SCDM power spectrum was calculated using the publicly available CMBFAST code (Seljak & Zaldarriaga 1996) and hence is COBE-normalised. For Model 1b we lowered the amplitude to reach a normalisation that agrees with the cluster abundance as described in Eke et al. (1996). All other models are based on Model 1a with no further modification to the amplitude than introduced by the artificially added feature. The modified power spectra follow the equation:

$$P_{\text{mod}}(k) = P(k) \cdot (1 \pm A \exp[-0.4(\frac{\log k - \log k_0}{\sigma_{\text{mod}}})^2]) \quad (1)$$

where $P(k)$ is the unmodified spectrum.

These features are completely Gaussian in log-space and can be described by their width σ_{mod} , height A , and the location k_0 of the bump (+) and dip (-), respectively. Their parameters are also summarised in Table 1. Each modification (characterised by the Model no. 2–6) was applied to the SCDM spectrum corresponding to Model 1a keeping the COBE normalisation fixed. A visual impression of the resulting power spectra can be found in Fig. 1 where all spectra are plotted (linearly extrapolated to redshift $z = 0.0$). These spectra are now used as an input to our initial conditions generator for the cosmological N -body simulations.

Again, we decided to use a COBE-normalised SCDM power spectrum as reference model because our intention was to investigate the influence of artificially introduced

Table 1. Specifications of the artificial modifications to the underlying Gaussian power spectra. The added features are of log-normal form, $\Lambda[e^\mu, \sigma^2]$. All modifications were superimposed onto an otherwise unmodified, COBE normalised SCDM model (Model 1a). The corresponding mass scale $M = \rho_{\text{crit}}\Omega \cdot \frac{4\pi}{3}(2\pi/k_0)^3$ is given in the last column.

label	$2\pi/k_0$	A	σ_{mod}	sign	mass scale
Model 1a					$\text{SCDM}, \Omega_0=1, h=0.5, \sigma_8=1.18$
Model 1b					$\text{SCDM}, \Omega_0=1, h=0.5, \sigma_8=0.52$
Model 2	$8 \text{ Mpc}/h$	3.00	0.10	+	$6 \cdot 10^{14} \text{M}_\odot/h$
Model 3	$8 \text{ Mpc}/h$	0.80	0.12	-	$6 \cdot 10^{14} \text{M}_\odot/h$
Model 4	$8 \text{ Mpc}/h$	0.95	0.48	-	$6 \cdot 10^{14} \text{M}_\odot/h$
Model 5	$16 \text{ Mpc}/h$	0.96	0.24	-	$5 \cdot 10^{15} \text{M}_\odot/h$
Model 6	$16 \text{ Mpc}/h$	0.96	0.48	-	$5 \cdot 10^{15} \text{M}_\odot/h$
OCDM					$\Omega_0=0.5, h = 0.7, \sigma_8=0.96$

features on scales corresponding to galaxy clusters (i.e. $8h^{-1}$ Mpc). For this reason we chose the COBE normalisation even though this SCDM model seems to be rather unattractive or even ruled out nowadays. However, by taking away power on cluster scales (as done for the majority of our 'feature' models) the value of σ_8 drops as we do not apply any re-normalisation of the power spectra. The purpose was not to find a new standard model which fits the observational data better but rather to analyse the influence of such features on an interesting range of cluster quantities; and this is more easily followed in a more distinctive structure formation scenario.

3 THE N-BODY SIMULATIONS

The simulations were carried out using Couchman's AP³M code (Couchman 1991). All simulations were performed with 128^3 particles in a box of side length $256h^{-1}$ Mpc; the (comoving) force resolution was fixed at $100h^{-1}$ kpc for all runs. We evolved the particle distribution from redshift $z = 30.0$ until $z = 0.0$ in 5000 steps. The box size was chosen such that the scales on which the Gaussian features had been added lie comfortably within the range covered by the simulations, e.g. our simulations cover the k-range from $k_{\text{min}} = 0.0245$ (limit set by box size) to $k_{\text{max}} = 1.571$ (limit set by particle number for representing the waves initially present), and the modifications lie clearly within that range (cf. Fig. 1). The particle-particle summation part of the AP³M code guarantees that we properly follow the evolution of all initially present waves especially for models 2–4 (cf. Couchman 1991).

For identifying particle groups within our numerical simulations we used the standard friends-of-friends algorithm (Davis et al. 1985) with the linking-lengths $ll = 0.2$ for the SCDM, and $ll = 0.17$ for the OCDM model, respectively (cf. Knebe & Müller 1999).

4 ANALYSIS

4.1 Power Spectrum Evolution

In Fig. 2 we plot the evolution of the dark matter power spectrum for models 1 through 6 (Model 1b and the OCDM model are left out for clarity as there is nothing unexpected

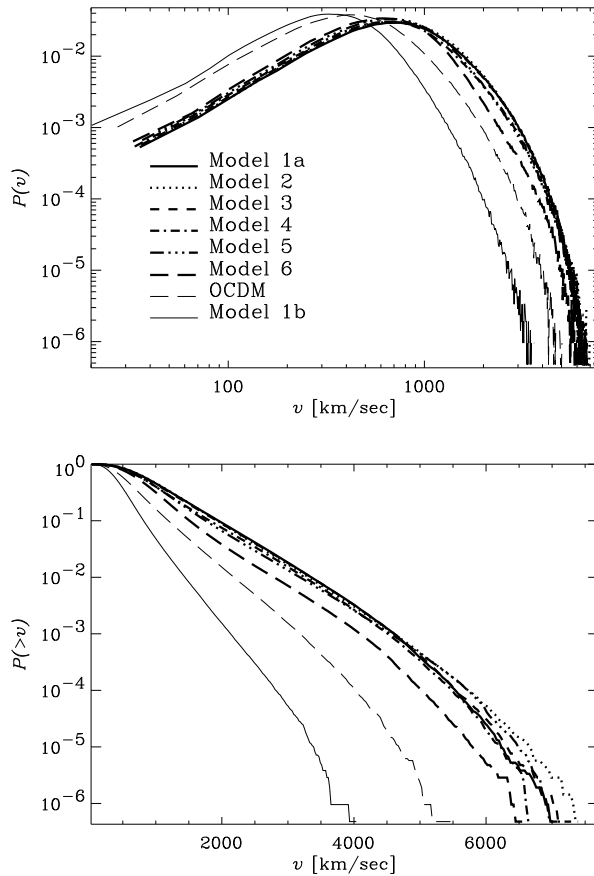


Figure 3. Velocity distribution for all dark matter particles

to observe). We see that the spectrum appears to be converging towards the unperturbed spectrum at late times. The feature nearly vanishes completely, leaving no further imprint in the power spectrum. The thin solid line crossing the whole plot corresponds to the unmodified, COBE-normalised SCDM spectrum linearly extrapolated to $z = 0.0$. Comparing it with the spectra derived from the numerical simulations, we notice a significant boost in power on small scales due to non-linear evolution. However, Model 6 with the very prominent dip at $16 h^{-1}$ Mpc nearly matches the linearly extrapolated SCDM power spectrum: at late times the non-linear boost of power almost exactly compensates the lacking power at the location of the dip.

We may conclude that even when starting with a prominent feature on small scales, there might only be little if any evidence for it left in the present universe when looking at the dark matter power spectrum $P(k)$. In any case, the *evolution* of the models *has* to be different, and one needs to think of other ways to investigate the influence of such features in the present day universe or to detect them in the evolution of $P(k)$ and related quantities. As far as the spectrum itself is concerned current galaxy clustering surveys offer little prospect of detecting these features in the evolution of $P(k)$. Observations of the Ly α forest, however, appear to be a promising tool for constraining $P(k)$ at high redshift (see e.g. Croft et al. 2000, Weinberg et al. 1998), particularly on the scales under investigation here.

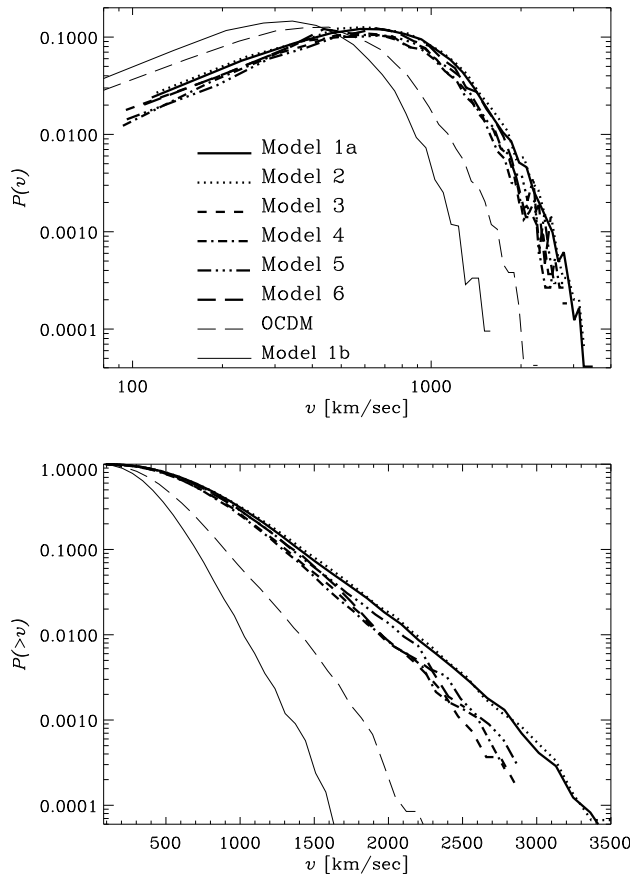


Figure 4. Velocity distribution for particle groups identified using a standard friends-of-friends algorithm with linking length 0.2. Only particles groups heavier than $2 \cdot 10^{13} h^{-1} M_{\odot}$ are taken into account.

4.2 Velocity Statistics

Next we consider the distribution of velocities for a) the dark matter particles and b) friends-of-friends particle groups. The peculiar velocity field results from the gravitational acceleration that develops from initial density fluctuations in the early universe. Clusters of galaxies can therefore be used as tracers of the large-scale peculiar velocity field (Bahcall, Cen & Gramann 1994).

In Fig. 3 we show the probability distribution $P(v)$ of dark matter particles with peculiar velocities in the range $v \pm dv$ along with the integrated distribution $P(> v)$. The same is plotted for friends-of-friends groups identified in all runs in Fig. 4. All curves are normalised by the total number of particles and total number of particle groups in the respective model. Here we also show the data for SCDM Model 1b as well as the fiducial OCDM model. Even though there are differences of a factor of two at the high velocity end of the distribution, it might be difficult to observationally distinguish these differences between modified and unmodified models.

The deviations between the cluster-normalised SCDM model and the COBE-normalised one are bigger than any differences between our 'feature' models. This deviation in velocities tending to lower values in the cluster-normalised

model can be explained by the lower value for σ_8 : the amplitudes of the initial density fluctuations are smaller and hence it takes longer to accelerate particles (and clusters) to high velocities; in the course of a simulation the velocity distribution function is always similar to a Maxwellian distribution whose peak gradually moves from low to high velocities. Apart from this we get increasingly more high velocity particles leading to a bigger 'tail' in the distribution. However, the most prominent difference is in the high velocity tail of the distribution for clusters. Only here it is possible to discriminate between models as our dip models show a significant drop in the integrated probability. We do not observe any galaxy clusters with peculiar velocities higher than 3000 km s^{-1} whereas there is a distinctive number of these objects in the unmodified Model 1a (and the bump Model 2). A detailed check showed that this tail is mainly due to objects with masses $M \lesssim 10^{14} h^{-1} M_{\odot}$. When only taking into account particle groups with heavier than $10^{14} h^{-1} M_{\odot}$ all curves for the 'feature' models fall on top of each other. However, the location and the width of the feature does not seem to have any significant influence.

4.3 The Masses of Galaxy Clusters

The most basic property of a galaxy cluster is its mass M . Nevertheless, this quantity can provide a lot of information especially when using the (cumulative) distribution of objects with a certain mass M ; and the evolution of the abundance of massive clusters within a given mass range is indeed one of the corner stones of the currently favoured Λ CDM model (Bahcall et al. 1999).

4.3.1 Mass Function and Press-Schechter Prediction

In Fig. 5 we show the cumulative mass function of particle groups for all our models at a redshift of $z = 0.0$. Even though we could not find well-pronounced imprints of the modifications in the power spectra at redshift $z = 0.0$ (cf. Fig. 2), we clearly see differences in the amplitude and slope of the cumulative mass function $n(> M)$. These deviations are mainly at the low mass end of the resolvable mass range, where a positive feature leads to an excessive number of objects and a negative feature to a lack of groups. This is in general agreement with an excess/lack of objects on mass scales corresponding to where the features are located. However, we always end up with the same number of galaxy clusters for masses $M > 10^{15} h^{-1} M_{\odot}$ (besides for Model 1b which shows too few massive groups due to the low normalisation). Unfortunately we are not able to resolve particle groups lighter than about $2 \cdot 10^{13} h^{-1} M_{\odot}$ and moreover, the simulation volume is still too small to get a statistically significant number of objects heavier than about $3 \cdot 10^{15} h^{-1} M_{\odot}$.

To check the validity of our results and get an impression of how they might generalise for larger/smaller mass objects we performed Press-Schechter (PS) calculations (Press & Schechter 1974) of the abundance of gravitationally bound objects. The (differential) number of objects for a given mass M can be calculated using their formula:

$$\frac{dn}{dM} dM = \sqrt{\frac{2}{\pi}} \frac{\bar{\rho}}{M} \frac{\delta_c}{\sigma_M} \left| \frac{d \ln \sigma_M}{d \ln M} \right| \exp \left(-\frac{\delta_c^2}{2\sigma_M^2} \right) \frac{dM}{M} \quad (2)$$

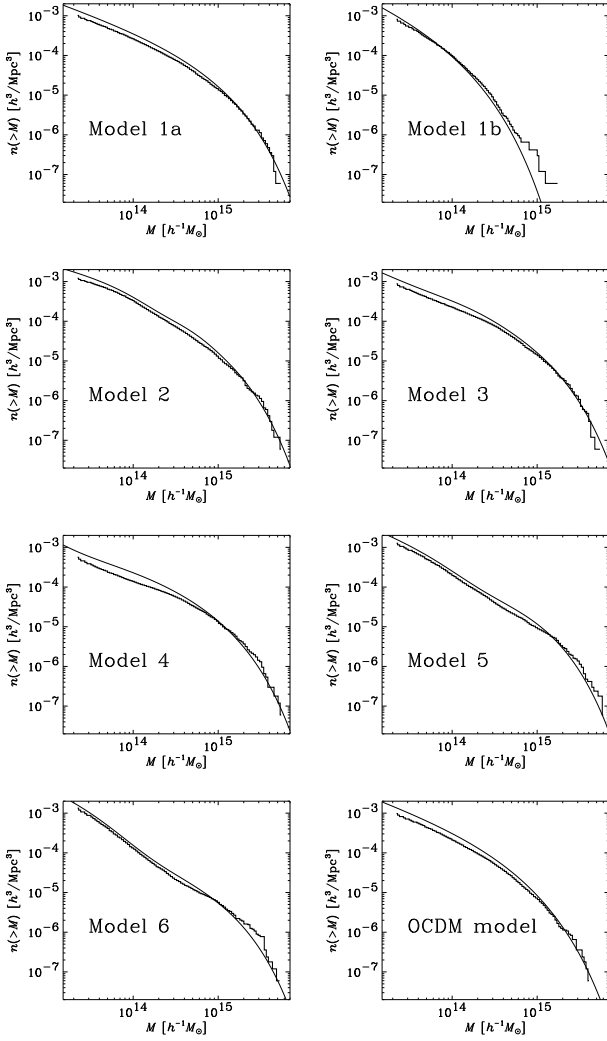


Figure 5. CDM mass function for redshifts $z = 0.0$ from simulations (histograms) and Press-Schechter prediction (thin lines).

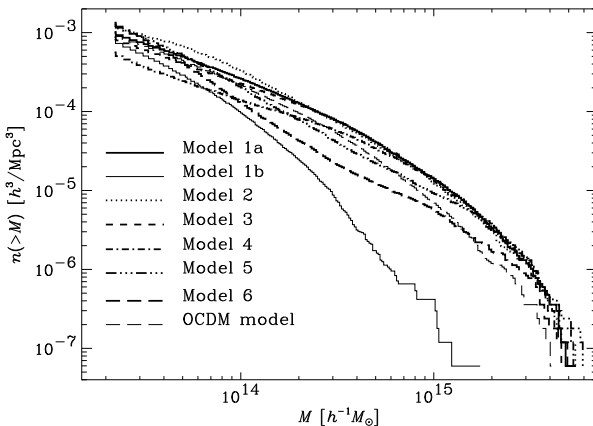


Figure 6. CDM mass functions as presented in Fig. 5.

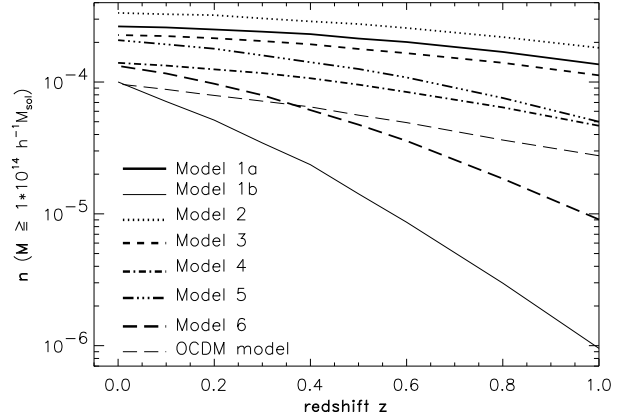


Figure 7. Evolution of SCDM cluster abundance.

with the variance σ_M defined as follows:

$$\sigma_M = \int P(k) W^2(kR) k^2 dk, \quad (3)$$

where $W(kR)$ is the window function (top-hat in our case) for filtering fluctuations in the power spectrum on scales characterised by R and hence mass $M = 4\pi R^3/3$. Using our model power spectra from Table 1 (plotted in Fig. 1) together with Eq. (3) and Eq. (2) we are able to compare our numerically achieved mass functions with the PS prediction. The results are shown in Fig. 5 as thin solid lines.

We observe a similar phenomenon as already seen in other comparisons of PS-predicted and N -body mass functions (Efstathiou et al. 1988, White, Efstathiou & Frenk 1993, Gross et al. 1998, Governato et al. 1999, Jenkins et al. 2001): the PS theory tends to show too many low mass objects (about a factor of 1.2) and too few high mass objects (again a factor of about 1.2). Apart from that the simulations agree fairly well with the Press-Schechter prediction, even in the cases where we modified the power spectra.

Anyway, to allow for better comparison between the individual models and the effect of the features on $n(> M)$ we also plot all mass functions derived from the numerical simulations (as already presented in Fig. 5) in one single Figure 6.

4.3.2 Evolution of the Cluster Abundance

The evolution of the cluster abundance has proven to be (potentially) one of the key constraints on the density parameter Ω_0 (e.g. Eke et al. 1996, Bahcall et al. 1997, Eke et al. 1998, Bahcall et al. 1999). This leads immediately to the question of how our modifications to the dark matter power spectrum influence this important issue. We have already seen that while we might not find hints in the observational power spectrum for the features under investigation, there are differences in the mass functions $n(> M)$. In Fig. 7 we show the evolution of galaxy clusters with mass M greater than $10^{14} h^{-1} M_\odot$.

The first thing that catches the eye is the difference between the COBE and cluster-normalised SCDM model when compared to the OCDM model. Only the cluster-normalised SCDM model shows a very steep evolution of the cluster

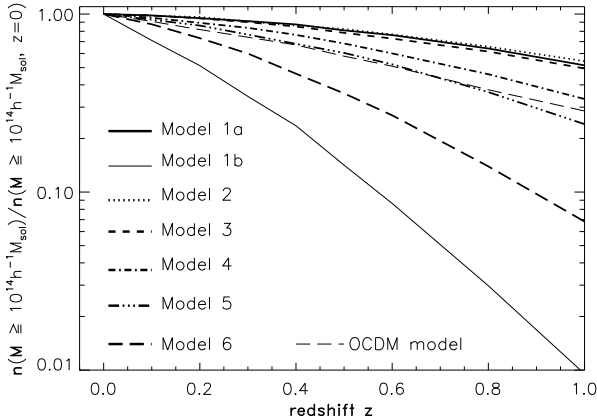


Figure 8. Evolution of SCDM cluster abundance normalised to unity at redshift $z = 0$.

abundance whereas the evolution in the COBE-normalised one agrees more or less with the OCDM model (cf. Bahcall, Fan & Cen 1997, Fig. 2 in their paper). It is now interesting to check whether our features affect only the normalisation of these evolutionary curves or also the slope. As we can see, the variations in the amplitude of the dip (or bump) mainly shift the cluster evolution up and down, and the location has an influence primarily on the slope of the curve.

This can be understood in the following way. Features on the $8h^{-1}$ Mpc scale are 'dynamically' important, in that this scale has evolved from the linear regime ($z \sim 1$) into quasi-linear or non-linear regime by now. Since the relative abundance of objects increases dramatically in the non-linear regime, we consequently expect still more (less) objects at late times if power had been added (subtracted) on the corresponding scale, i.e. features on this scale are expected to affect the shape of the abundance evolution of corresponding mass objects. Conversely, features that up to present have remained in the linear regime only add (subtract) power on dynamically unimportant scales, thus only affecting the normalisation. *

Moving the dip from the non-linear scale of $8h^{-1}$ Mpc to the semi-linear $16h^{-1}$ Mpc mainly results in an overall lack of power and therefore we expect the cluster evolution to be closer to the cluster-normalised ($\sigma_8 = 0.52$) Model 1b. However, the evolution for Model 4 agrees fairly well with the OCDM Model. This can be seen even better in Fig. 8 where we normalised the cluster abundance at redshift $z = 0$ to unity for all models to allow for better comparison of the slopes of the curves.

A similar effect was already observed by Barriga et al. (2000) where the influence of a step-like feature in the primordial power spectrum was studied in the context of phase transitions during inflation. However, their features are on larger scales and thus would leave traces in current epoch measurements of the CMB and large scale structure.

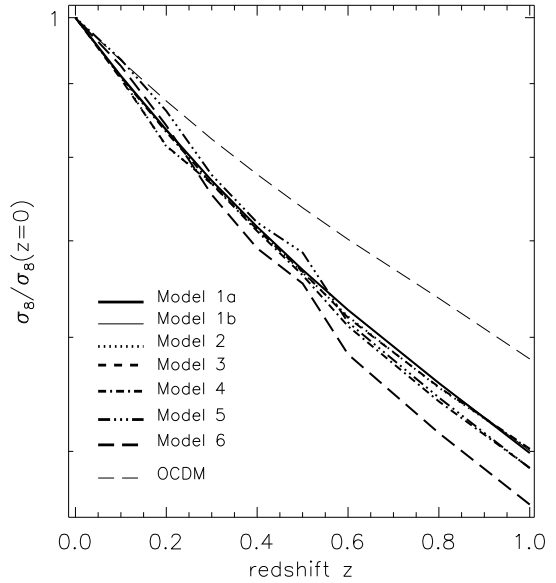


Figure 9. Evolution of σ_8 in all models. The evolution in all models is normalised to be unity at redshift $z = 0$.

4.4 σ_8 Evolution

As the number of objects formed depends on the normalisation of the input power spectrum measured via σ_8 (cf. Eq. 3), it is interesting to check the evolution of this quantity with redshift, too. Fig. 9 shows this evolution for all models. Again, all curves are normalised to the value at redshift $z = 0$ to allow for better comparison of the slopes. We observe no overlap of any feature model with the OCDM model: regarding the evolution of the dark matter fluctuations measured in $8h^{-1}$ Mpc spheres (rather than the cluster evolution) the OCDM model still differs significantly from all other models. Moreover, it is difficult again to distinguish between our feature models as well as the differently normalised SCDM models itself. Only Model 6 shows a steeper evolution from redshift $z \sim 1$ to $z \sim 0.5$. Hence σ_8 -evolution does not provide a discriminant of features in the power spectrum. However, Robinson, Gawiser and Silk (2000) have shown that σ_8 and cluster abundance combine to probe non-gaussianity.

4.5 Halo-Halo Correlation

In Fig. 10 we present the halo-halo correlation function for our models. We fixed the number density to $n = 5 \cdot 10^{-4} h^3 \text{Mpc}^{-3}$ which actually means to only use the $N = n \cdot V$ most massive halos with $V = 256h^{-1}$ Mpc being our simulation volume.

We now observe more obvious differences between these models, which can be fully ascribed to our artificial modifications of the initial power spectrum. The amplitude of the cluster correlation function is actually insensitive to the amplitude of fluctuations in the density field (Croft & Efstathiou 1994), which is clearly reflected when comparing Model 1a and 1b. Moreover, there are also only moderate changes in the cluster correlation function when varying the

* Though, if the difference in power is very large (c.f. abundance evolution for $\sigma_8 = 1.18$ and $\sigma_8 = 0.52$) there is a significant change in the slope of the abundance evolution, too.

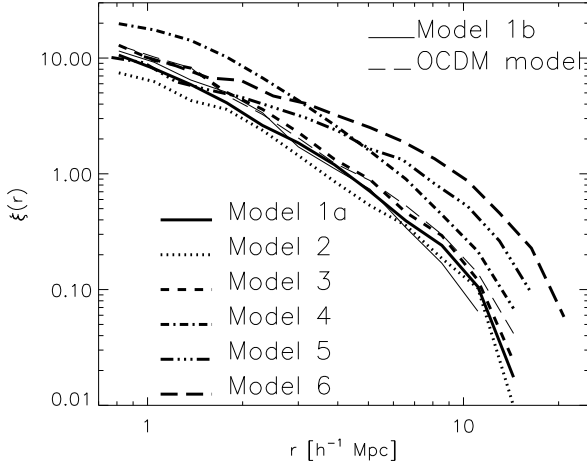


Figure 10. Halo-Halo correlation function for particle groups. The number density of objects was fixed in all models to $n = 5 \cdot 10^{-4} h^3 \text{Mpc}^{-3}$.

cosmological parameters from our SCDM Model 1a/b to the OCDM model (cf. Martel & Matzner 2000). But as we move on to our feature models not only the amplitude of the correlation function increases (for the dip models), but also the slope changes (i.e. Model 6). This suggests a strongly (and non-linearly) biased formation of galaxy clusters in those models compared to a 'normal' SCDM model.

As there was no obvious biasing observed in the dark matter power spectrum (which is nothing more than the Fourier transform of the dark matter correlation function), the effect seen in Fig. 10 is entirely due to a different cluster formation scenario in our dip models. This is caused by the fact that by adding (subtracting) power only on a certain scale the relative strength of different waves becomes more and more important. If we put less power into high- k waves (i.e. Model 3 and 4) but leave the largest waves unmodified we eventually bias the formation process of galaxy clusters with respect to an unmodified SCDM model as can be observed in Fig. 10. Massive clusters indeed are highly biased, and the extent to which one may have difficulty in accounting for this in standard low density models may constitute the strongest signature of a possible feature at redshift $z = 0$ in a SCDM model.

4.6 Density Profiles

We have already seen that we introduced a strong bias in the cluster formation process by altering the ratio of high- to low- k waves amplitudes. This immediately raises the question of whether this will subsequently lead to deviations in the shapes of the clusters themselves. We have therefore calculated the density profiles for massive FOF groups ($M > 10^{15} h^{-1} \text{M}_\odot$) and show the results for a representative high-mass halo $M \sim 3.5 \cdot 10^{15} h^{-1} \text{M}_\odot$ (~ 1700 particles) in Fig. 11. The curves for models 2 through 6 have been shifted upwards by successive factors of 2, whereas the OCDM profile was lowered by a factor of 2.

We can see that modifying the power spectrum does not affect the slope and amplitude of the density profiles.

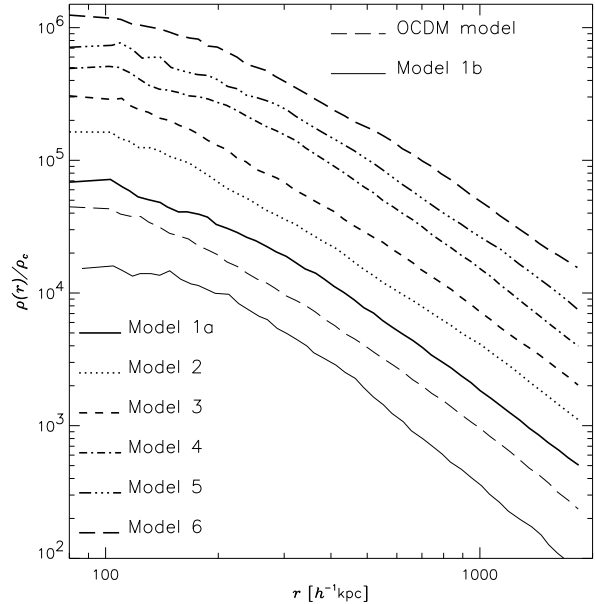


Figure 11. Density profile for one halo in all models.

Only the SCDM model 1b deviates from the other curves as the corresponding halo consists of only about 500 particles. Due to the resolution limits of our simulations, we are not able to quantify the substructure content of these galaxy clusters in more detail as the most massive objects contain 'only' 2000-2500 particles. But a visual comparison of the particle distributions in those clusters provided no obvious differences.

5 ANALYTICAL ESTIMATES

We have seen above that SCDM models with features at small scales may display an evolution of their cluster abundance that is similar to that in the OCDM model to within some constant offset in amplitude. The question remains of how far we can push this agreement and to what extent this also holds for cluster masses larger than the ones we were able to investigate numerically. To this end we performed Press-Schechter (Press & Schechter 1974) calculations to investigate a larger set of models. However, since we are considering the evolution of cluster abundances, this also requires a relation for the redshift dependence of the critical overdensity δ_c , which is left unspecified in the original PS approach. We determined approximate relations for the unmodified SCDM and OCDM models by matching their cluster abundance evolution to that of the corresponding N-body simulations:

$$\delta_c^{SCDM}(a) = 1.2 + 0.6a, \quad \delta_c^{OCDM}(a) = 1.45 + 0.3a \quad (4)$$

where $a = 1/(1+z)$ is the cosmic scale factor at redshift z .

For the OCDM model the δ_c relation almost exactly reproduces the abundance evolution. The corresponding relation for the SCDM model was rather chosen to fit both unmodified SCDM and featured SCDM models reasonably well, matching the N-body evolution to within 10 percent for the unmodified SCDM model, typically to within 20 percent

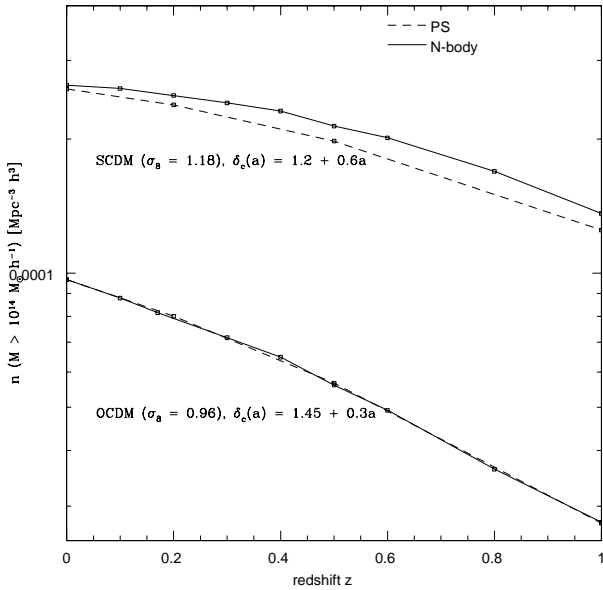


Figure 12. Comparison of evolution of clusters of mass $M > 10^{14} M_{\odot} h^{-1}$ in simulations and PS using the relations for δ_c from the simulations.

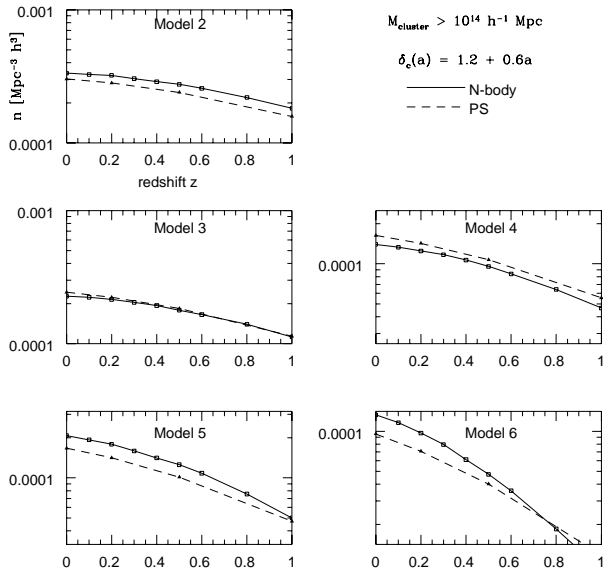


Figure 13. Comparison of abundance evolution for clusters with mass $M > 10^{14} M_{\odot} h^{-1}$ in simulations and PS. All PS calculations use $\delta_c(a) = 1.2 + 0.6a$ (eq (4)).

for models 2 to 5 and 30 percent for model 6. This is shown in figures 12 and 13. An accurate fit to the unmodified SCDM model only would have required $\delta_c(a) = 1.25 + 0.5a$.

However, the agreement between N-body and PS data should be viewed with care, particularly when large sharp features are included: At the location of the features, we essentially introduce a more rapidly changing spectral index. This might contribute to a larger discrepancy between N-

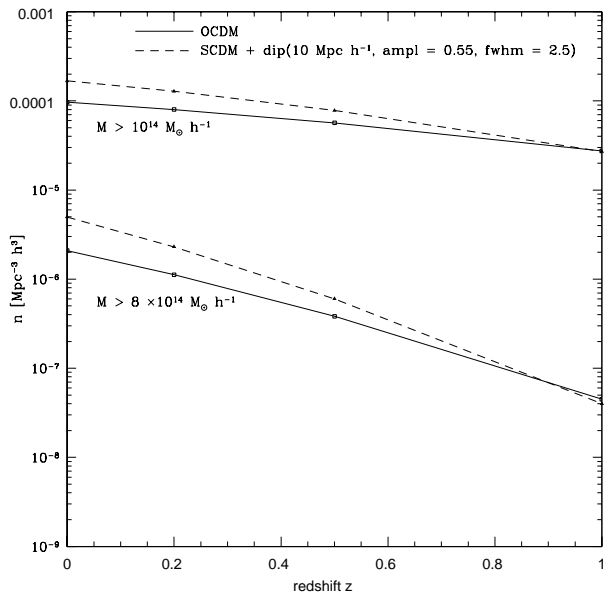


Figure 14. PS calculations of abundance evolution for OCDM and SCDM with a broad dip at $10 \text{ Mpc } h^{-1}$. For the mass cuts the two agree to within less than a factor of 2 and 3 respectively across the whole redshift range.

body and PS data. To our knowledge agreement between PS and numerical simulations has so far only been established for power spectra with constant (power law) or slowly varying (e.g. SCDM) spectral indices - it is not obvious why this should also hold when a sharply varying index is being introduced, particularly on scales that only now turn non-linear. In the following, however, we will assume that this is not a problem and use the δ_c^{SCDM} relation from equation (4) as a best estimate for PS predictions of the abundance evolution for other small scale features in the SCDM model. We also assume that the δ_c relation for OCDM describes the abundance evolution in higher mass cuts as well as it does for $M > 10^{14} h^{-1} M_{\odot}$ in our simulations.

As seen above, one might expect that adding (subtracting) power only at specific scales leads to a larger (smaller) abundance of objects with mass corresponding to these scales. This is not obvious for scales that are already in the non-linear regime, as we have a coupling across scales, and also objects not only get newly created but now have also been partly incorporated into larger objects, i.e. the effect of a feature on a specific scale spreads out, not only in the evolution of the power spectrum as we have seen above, but also in the abundance of objects of corresponding mass. However, for broad features we may assume that the latter is less important, since a whole range of scales and corresponding masses are affected.

To check this, we placed a broad Gaussian dip in the SCDM model ($A = -0.55$, $\sigma_{\text{mod}} = 2.5$) at $10 h^{-1} \text{ Mpc}$, which is expected to affect a similarly broad range of masses centred on $M \sim 10^{14} - 10^{15} M_{\odot} h^{-1}$. A broad feature of this kind is naturally generated by e.g. including a running spectral index term when expanding the primordial perturbation spectrum (Hannestad, Hansen & Villante 2000).

Comparing Fig. 12 with Fig. 14 confirms that the abundance of masses in these ranges ($M > 10^{14}$, $M > 8 \cdot 10^{14} h^{-1} M_\odot$, the mass range covered by e.g. Bahcall & Fan 1998) is significantly suppressed. What is more, the abundance evolution for the mass cuts agrees in logarithmic slope and magnitude with that in the OCDM model to within a factor of less than two and three across all redshifts up to $z = 1$ for the lower and upper mass cuts respectively.

Given that observations of the most distant massive clusters currently only constrain the abundance to within one or two orders of magnitude (see e.g. Bahcall & Fan 1998), SCDM with broad features towards small scales, mimicking (in shape and absolute magnitude) the abundance evolution expected in OCDM models, can therefore not be ruled out. A similar result is obtained by Barriga *et al.* (2001) who consider primordial step-like features in the context of phase transitions during inflation, however their features are on larger scales in the linear regime and thus would also leave traces in current epoch measurements of the CMB and large scale structure.

6 CONCLUSIONS

In this paper we presented a series of simulations all based on the COBE normalised SCDM model but with Gaussian features added to an otherwise unperturbed power spectrum (called 'feature' models). Such bumps (or dips) might naturally arise from non-standard inflationary theories and our main purpose was to investigate their influence on the large-scale structure of the Universe as measured via galaxy clusters. We analysed the evolution of the dark matter power spectrum, the large-scale velocity field represented by the velocity distribution of galaxy clusters, the evolution of the cluster abundance, the halo-halo correlation function, and density profiles of clusters. We furthermore compared our numerical results to analytical predictions based on the Press-Schechter formalism (Press & Schechter 1974).

When comparing the modified SCDM models to a fiducial OCDM model, we can see that when choosing an appropriate scale for the added feature the histories of cluster abundance evolution might be indistinguishable. However, there is still a discrepancy in the overall normalisation left at the present epoch, with only the slopes of the cluster abundance evolution coinciding. But as observations of the most distant massive clusters only constrain the current abundance to within one or two orders of magnitude (cf. Bahcall & Fan 1998), an SCDM model including such a broad feature cannot be ruled out.

Finally we remark that whatever the origin or nature is of these bumps and dips, their effect on the evolutionary history of the SCDM model is much more moderate than changes in the cosmological parameters of the model itself, e.g. lowering the normalisation from $\sigma_8 = 1.18$ (COBE normalisation) to $\sigma_8 = 0.52$ (cluster normalisation). It is therefore an observational challenge to find traces of such features, and the best place to search for them might be the cluster-cluster correlation function which appears to be highly biased with respect to the 'normal' SCDM model. This is due to an unusual ratio of power for high- and low- k waves, which will be reflected in the aforementioned 'more than biased' cluster formation scenarios.

ACKNOWLEDGEMENTS

We are grateful to the referee Mirt Gramann for helpful comments and suggestions. We also acknowledge the use of Hugh Couchman's AP³M code. RRI gratefully acknowledges a Graduate Studentship from Oxford University and support from St Cross College, Oxford.

REFERENCES

Bahcall N.A., Cen R., Gramann M., ApJ Lett. **430**, 13 (1994)
 Bahcall N.A., Fan X., Cen R., ApJ Lett. **485**, 53 (1997)
 Bahcall N.A., Fan X., ApJ **504**, 1 (1998)
 Bahcall N.A., Ostriker J.P., Perlmutter S., Steinhardt P.J., Science **284**, 1481 (1999)
 Barriga J., Gaztanaga E., Santos M.G., Sarkar S., astro-ph/0011398 (2000)
 Broadhurst T.J., Ellis R.S., Koo D.C., Szalay A.S., Nature **343**, 726 (1990)
 Chung D.J.H., Kolb E.W., Riotto A., Tkachev I.I., hep-ph/9910437 (1999)
 Couchman H.M.P., ApJ Lett. **368**, 23 (1991)
 Croft R.A.C. & Efstathiou G., MNRAS **267**, 390 (1994)
 Croft R.A.C., Weinberg D.H., Bolte M., Burles S., Hernquist L., Katz N., Kirkman D., Tytler D., astro-ph/0012324 (2000)
 Davis M., Efstathiou G., Frenk C.S., White S.D.M., ApJ **292**, 371 (1985)
 Efstathiou G., Frenk C.S., White S.D.M., Davis M., MNRAS **235**, 715 (1988)
 Eke V.R., Cole S., Frenk C.S., MNRAS **282**, 263 (1996)
 Einasto J., Einasto M., Gottlöber S., Müller V., Saar V., Starobinsky A.A., Tago E., Tucker D., Andernach H., Frisch P., Nature **385**, 139 (1997)
 Eke V.R., Cole S., Frenk C.S., Henry J.P., MNRAS **298**, 1145 (1998)
 Gaztanaga E., Baugh C.M., MNRAS **294**, 229 (1998)
 Governato F., Babul A., Quinn T., Tozzi P., Baugh C.M., Katz N., Lake G., MNRAS **307**, 949 (1999)
 Griffiths, L., Silk, J., Zaroubi, S. astro-ph/0010571
 Gross M.A.K., Somerville R.S., Primack J.R., Holtzmann J., Klypin A.A., MNRAS **301**, 81 (1998)
 Hamilton A., Tegmark M., astro-ph/0008392
 Hannestad S., Hansen S.H., Villante F.L., astro-ph/0012009
 Jenkins A., Frenk C.S., White S.D.M., Colberg J.M., Cole S., Evrard A.E., Couchman H.M.P., Yoshida N., MNRAS **321**, 372 (2001)
 Knebe A., Müller V., A&A **341**, 1 (1999)
 Lange A.E., Phys. Rev. D**63**, 1 (2001)
 Lesgourges J., Polarski D., Starobinsky A.A., MNRAS **297**, 769L (1998)
 Lidsey J.E., Liddle A.R., Kolb E.W., Copeland E.J., Barreiro T., Abney M., Rev. Mod. Phys. **69**, 373, (1997)
 Martel H., Matzner R., ApJ **530**, 525 (2000)
 Martin J., Riazuelo A., Sakellariadou M., astro-ph/9904167 (1999)
 Press W.H., Schechter P., ApJ **187**, 425 (1974)
 Robinson, J. Gawiser, E., Silk, J., ApJ **539**, 89 (2000)
 Seljak U., Zaldarriaga M., ApJ **469**, 437 (1996)
 Weinberg D.H., Burles S., Croft R.A.C., Davé R., Gomez G., Hernquist L., Katz N., Kirkman D., Liu S., Miralda-Escudé J., Pettini M., Phillips J., Tytler D., Wright J., Proceedings: Evolution of Large Scale Structure - Garching, August 1998, astro-ph/9810142
 White S.D.M., Efstathiou G., Frenk C.S., MNRAS **262**, 1023 (1993)